Effects of snow physical parameters on shortwave broadband albedos

Teruo Aoki
Meteorological Research Institute, Tsukuba, Japan

Akihiro Hachikubo
Kitami Institute of Technology, Kitami, Japan

Masahiro Hori
Japan Aerospace Exploration Agency, Tokyo, Japan

Received 16 February 2003; revised 28 May 2003; accepted 11 June 2003; published 14 October 2003.

[1] Snow pit work of several-day intervals was performed simultaneously with radiation budget observations during two winters in eastern Hokkaido, Japan. From these data we investigated the effects of elapsed time after snowfall (snow aging), air temperature, snow surface temperature, snow grain size, and snow impurities on the visible and the near infrared albedos for improving the snow albedo scheme in the land surface process from an empirical model to a physically based model. The dependence of albedos on elapsed time after snowfall could be clearly classified by dividing the snow-covered period into a dry snow season and a wet snow season rather than by snow surface temperature. The albedo reduction by snow aging statistically depends on the snow surface temperature, which is often used to predict the snow albedo in the empirical model of land surface process. However, the albedo reduction rate was very scattered for snow surface temperatures above −10°C. This is because the snow albedo reduction essentially depends on the snow grain size and the concentration of snow impurities. Using the radiative transfer model for the atmosphere-snow system, the effects of these snow physical parameters on broadband albedos are calculated and compared with the observed ones. The measured broadband albedos fell close to the range of theoretically calculated ones as functions of these snow physical parameters. In particular, the measured near infrared albedo agreed well with the theoretically calculated ones both for the dependence of snow grain size and snow impurities but not as well for the visible albedo in detail. In the near infrared region the light absorption by ice is strong, and thus the snow albedo contains the information of snow physical parameters near the surface where these parameters are measured. In contrast, the visible albedo contains the snow information in the deeper layer because the ice is relatively transparent in the visible region. This suggests the necessity of the multiple-snow-layer model for the visible region in the physically based snow albedo model. *INDEX TERMS:* 0305 Atmospheric Composition and Structure: Aerosols and particles (0345, 4801); 1719 History of Geophysics: Hydrology; 1863 Hydrology: Snow and ice (1827); 3322 Meteorology and Atmospheric Dynamics: Land/atmosphere interactions; 3359 Meteorology and Atmospheric Dynamics: Radiative processes; *KEYWORDS:* broadband albedo, snow physical parameter, radiative transfer

Citation: Aoki, T., A. Hachikubo, and M. Hori, Effects of snow physical parameters on shortwave broadband albedos, *J. Geophys. Res.*, *108*(D19), 4616, doi:10.1029/2003JD003506, 2003.

1. Introduction

[2] The cryosphere is very sensitive to global warming because the surface albedo in the cryosphere drastically changes due to a phase change of snow/ice surfaces. According to the report of *Intergovernmental Panel for Climate Change* (*IPCC*) [2001], many general circulation models (GCMs) predict a large warming in the high latitudes of the Northern Hemisphere in this century, which is related to the reduced snow and sea ice cover. In the Northern Hemisphere, the snow cover extent has decreased about 10% since 1966, and the sea ice extent has decreased 2.8 ± 0.3% per decade since 1978 [*IPCC*, 2001]. Both measurements are based on satellite data analyses for snow cover extent [*Robinson*, 1997] and sea ice extent [*Parkinson et al.*, 1999; *Johannessen et al.*, 1995]. A large positive trend of surface air temperature exceeding 1.0°C per decade for land at high latitudes in the Northern Hemisphere, in winters from 1976 to 2000 [*IPCC*, 2001], is also estimated from the analysis by *Jones et al.* [2001].

Copyright 2003 by the American Geophysical Union.
0148-0227/03/2003JD003506$09.00

[3] Surface conditions in the cryosphere have thus changed in the past several decades and are expected to change in the future. To accurately simulate the future climate in the cryosphere, a better land-surface process scheme, especially with an accurate snow albedo model, is necessary. For sea ice, the snow albedo is important because large parts of the sea ice surface are covered by snow. The factors to change the spectral albedo of the snow surface are essentially divided into two categories: (1) the physical parameters of snow and (2) the external parameters such as atmospheric conditions and solar zenith angle [*Aoki et al.*, 1999]. The important factors in the snow physical parameters are snow grain size and concentration of snow impurities. The near infrared albedo decreases with an increase of snow grain size [*Wiscombe and Warren*, 1980], and the visible albedo is reduced by snow impurities [*Warren and Wiscombe*, 1980]. Under clear-sky conditions, the monochromatic snow albedo has a solar zenith angle dependence (high at a large solar zenith angle and vice versa). *Warren* [1982] explained this phenomenon by an extinction of the direct solar beam in the snow and an extreme asymmetry of the scattering phase function of snow particles. Under cloudy conditions, the direct beam disappears and the snow surface is illuminated diffusely, so the monochromatic albedo loses solar zenith angle dependence and becomes almost constant at a solar zenith angle of 50° for a clear sky. In this case, the spectrally integrated albedo also loses its solar zenith angle dependence, while the value is higher than those at any solar zenith angle for a clear sky [*Aoki et al.*, 1999]. *Liljequist* [1956] explained this by the difference in the spectral distribution of the downward solar flux between the clear and cloudy sky cases. For areas of sufficiently deep and flat snow, such factors as snow grain size, concentration of snow impurities, sky condition, and solar zenith angle are essentially the dominant factors for the change of spectral snow albedo (thus broadband albedo as well).

[4] To estimate snow albedo accurately, the factors mentioned above should be dealt with explicitly in land surface models (LSMs) or GCMs. However, the snow submodels estimating albedo empirically are mainly used in the present LSMs or GCMs. For example, in the simple biosphere model (SiB) by *Sellers et al.* [1986] the surface albedo of snow with a water equivalence greater than 0.01 m is assumed to be a fixed value of 0.8 (0.4) for the visible (near infrared) wavelength region. These values are reduced to 60% of original values when the surface temperature is close to or at the melting point. The snow submodel in the Biosphere-Atmosphere Transfer Scheme (BATS) by *Dickinson et al.* [1986, 1993] is a somewhat complicated empirical model in which three effects were taken into account to estimate snow albedo: (1) calculating the albedos in the visible ($\lambda < 0.7$ μm) and the near infrared ($\lambda \geq 0.7$ μm) spectral regions separately; (2) solar zenith angle dependence; (3) snow aging dependent on the snow surface temperature, in which the snow aging effect contains the implicit effects of snow grain growth and impurities. *Roesch et al.* [1999] also employed the dependence of snow albedo on surface temperature, in which surface albedo is interpolated between fixed albedos at temperatures of 0°C and −10°C for the three types of surfaces (land snow, land ice, and sea ice). Recently, in community of land modeling groups the common land model (CLM) has been developed [*Dai et al.*, 2003] and has already been coupled with the National Center for Atmospheric Research (NCAR) Community Climate Model (CCM3) [*Zeng et al.*, 2001]. Although many processes were improved in CLM, snow albedo process is basically the same as that in BATS (Y. Dai et al., Common Land Model (CLM) technical documentation and user's guide, 69 pp., 2001, available at http://climate.eas.gatech.edu/dai/clmdoc.pdf).

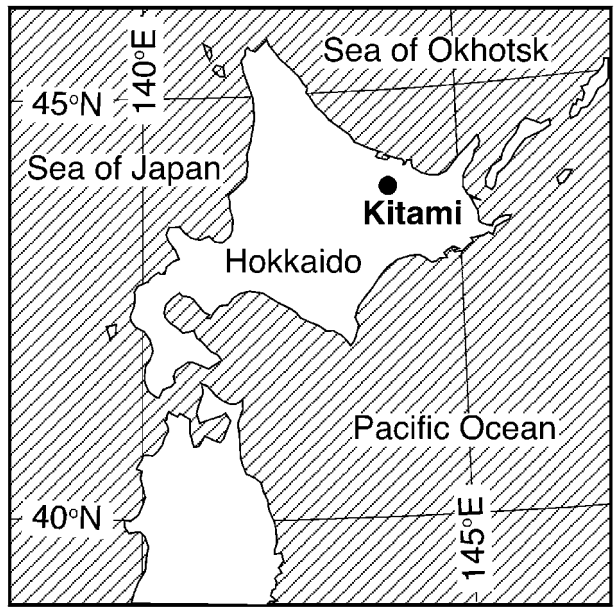

Figure 1. Map of observation site (43°49′21″N, 143°54′13″E, 94 m above sea level), location of the meteorological observation field of the Kitami Institute of Technology.

[5] In the last several years, some snow albedo models were validated using long-term surface meteorological data. *Yang et al.* [1997] verified the performance of the snow submodel in BATS model using the long-term snow data from the former Soviet Union and arrived at a good agreement for snow albedo. *Takayabu et al.* [2001] compared the performance of four kinds of LSMs (JMA-SiB, CCSR/NIES-LAND, MATSIRO, and TOHKU) with the GEWEX Asian Monsoon Experiment (GAME)/Tibet data and concluded that the forecasted snow masses are very different because of the differences in the snow albedo schemes. Two models (JMA-SiB and MATSIRO) change the snow albedo depending on the snow surface temperature as *Roesch et al.* [1999]; the other two models consider the effect of snow aging. *Mabuchi et al.* [1997] reduce the albedo exponentially depending on the elapsed time after snowfall. *Yamazaki* [2001], in the less improved version of TOHOKU, introduced the empirical air temperature dependence into the albedo reduction (snow aging) rate. In this way, the empirical snow albedo models have been widely used. However, the parameters used in such empirical models should differ for time and place, especially for future climate conditions.

[6] Parameterization of snow albedo in GCM by *Marshall and Oglesby* [1994] is one of the very few physically based snow albedo models that take into account

the effects of snow grain size, the concentration of snow impurities, the diffuse fraction of the downward solar flux, and the solar zenith angle. Their model is based on the theoretically calculated snow albedo model of *Wiscombe and Warren* [1980]. *Marshall and Oglesby* [1994] emphasized the necessity for snow hydrology based on fundamental physical processes for simulating climates with confidence. *Nolin and Frei* [2001] calculated the energy budget on the snow surface using the same albedo parameterization by snow grain size. They reported that the variable albedo was significantly more realistic and representative than the constant albedo value. Since the empirical snow models generally contain the tuning parameters or experimental coefficients determined by specific observations, this would cause an error in estimated albedos for global application. A physically based snow albedo model is expected to solve this problem. However, there is no direct comparison of parameters such as snow grain size or concentration of snow impurities with snow albedos from long continuous observations. Therefore we performed snow pit work of several-day intervals simultaneously with radiation budget and meteorological observations during two winters in eastern Hokkaido, Japan. From these data, we investigated the effects of time after snowfall (aging), snow surface temperature, impurities, and grain size on the visible, the near infrared, and the shortwave (total) albedos.

2. Instrumentation and Data

2.1. Radiation Budget and Meteorological Components

[7] In the radiation budget observation, the upward and downward components of radiant flux densities in shortwave (λ = 0.305–2.8 μm), near infrared (λ = 0.695–2.8 μm), and longwave (λ > 4 μm) spectral regions were measured using four pyranometers (MS-801) and two pyrgeometers (MS-200) made by EKO Instruments Trading Co., Ltd. (Japan). For measuring the near infrared region, a cutoff filter dome at λ = 0.695 μm was installed on the pyranometer. Each radiation component was sampled every 10 s, and 1-min-averaged values were stored in a data logger. The visible radiation was determined by subtracting the near infrared radiation from the shortwave radiation. Broadband albedos were calculated from 30-min-averaged values of measured radiation components at every half-hour interval (01–30 and 31–00 in minutes). We analyzed only the data nearest to the local solar noon (the data measured during 1131–1200 LT) to keep the observational condition uniform. Otherwise, when the sun is at an easterly or westerly position, the snow surface is shadowed by the two vertical frames supporting the instruments. In early morning, frost sometimes formed on the instruments set upward in the 1999/2000 winter. (In the 2000/2001 winter, a ventilation system on the glass dome was employed to remove the frost). In such cases, the data measured before we removed the frost in the morning might be erroneous. We limited the data to be analyzed to a snow depth of more than 30 cm, which is sufficiently deep optically, and thus the surface albedo is not influenced by the underlying surface (except as discussed in Figures 2 and 5). Although we need to investigate the effects of snow physical parameters on albedo, the conditions of the solar zenith angle and cloud cover at local solar noon, which could affect the snow albedo as mentioned in section 1, also vary during the observation period. We will discuss how much these factors deviate from the broadband albedos that use a multiple scattering radiative transfer model for the atmosphere-snow system in Appendix A.

[8] Meteorological components measured with the radiation budget observation were air temperature and relative humidity at a height of 1 m above the snow surface. These data were recorded every minute in a data logger. Snow depth was measured with a laser snow gauge, and precipitation with a rain gauge, every hour. The snow surface temperature was calculated from the observed longwave radiation data using the equation given by

$$T_S = \left(\frac{LW^{\uparrow} - (1-\varepsilon)LW^{\downarrow}}{\varepsilon\sigma}\right)^{\frac{1}{4}}, \qquad (1)$$

where $LW^{\downarrow}$ and $LW^{\uparrow}$ are downward and upward longwave flux densities, ε is snow emissivity for which we employed the value of 0.97 [*Kondo and Yamazawa*, 1986], and σ is the Stefan-Boltzmann constant.

2.2. Snow Pit Work

[9] Snow pit work was done two or three times per week for the components of snow type, temperature, density, and snow grain size in each snow layer, together with snow sampling for the measurement of snow impurities. In the measurements of snow grain size, two or three kinds of dimensions at the snow surface were measured with a handheld lens by the same method as *Aoki et al.* [2000]. These measurements were one-half length of the major axis of crystals or dendrites (r_1), one half the branch width of dendrites or one half the dimension of the narrower portion of broken crystals (r_2), and one half the crystal thickness only for dendrites or plate-like crystals (r_3). For aggregate granular grains, one half the dimension of the cluster and each grain's diameter were measured as r_1 and r_2. *Aoki et al.* [1998, 2000] concluded that the optically equivalent snow grain size was r_2 for new snow or faceted crystals from the spectrally detailed albedo measurements together with snow pit work. The snow impurities (water-dissolved solid particles in the snowpack) were filtered using a Nuclepore filter, after melting the snow sample. We used a two-stage filtering system of Nuclepore filters with different pore sizes of 0.2 μm and 5.0 μm for snow samples from the surface to three snow depths (0–1 cm, 0–5 cm, and 0–10 cm). This produced rough information of the impurity types and a vertical profile of the impurities in the snow. We found the majority of impurities were collected on the Nuclepore filter with a pore size of 5.0 μm, and the main constituent was mineral particles. The concentrations of snow impurities were estimated by direct measurements of the weights of Nuclepore filters, before and after filtering, using a balance.

3. Observation Conditions

[10] All field measurements were carried out in the 1999/2000 and 2000/2001 winters at the meteorological observation field (43°49′21″N, 143°54′13″E, 94 m above sea level) of Kitami Institute of Technology in eastern Hokkaido, Japan (Figure 1). The surface condition for the snow-free period was flat with withered grass. Figure 2 shows the

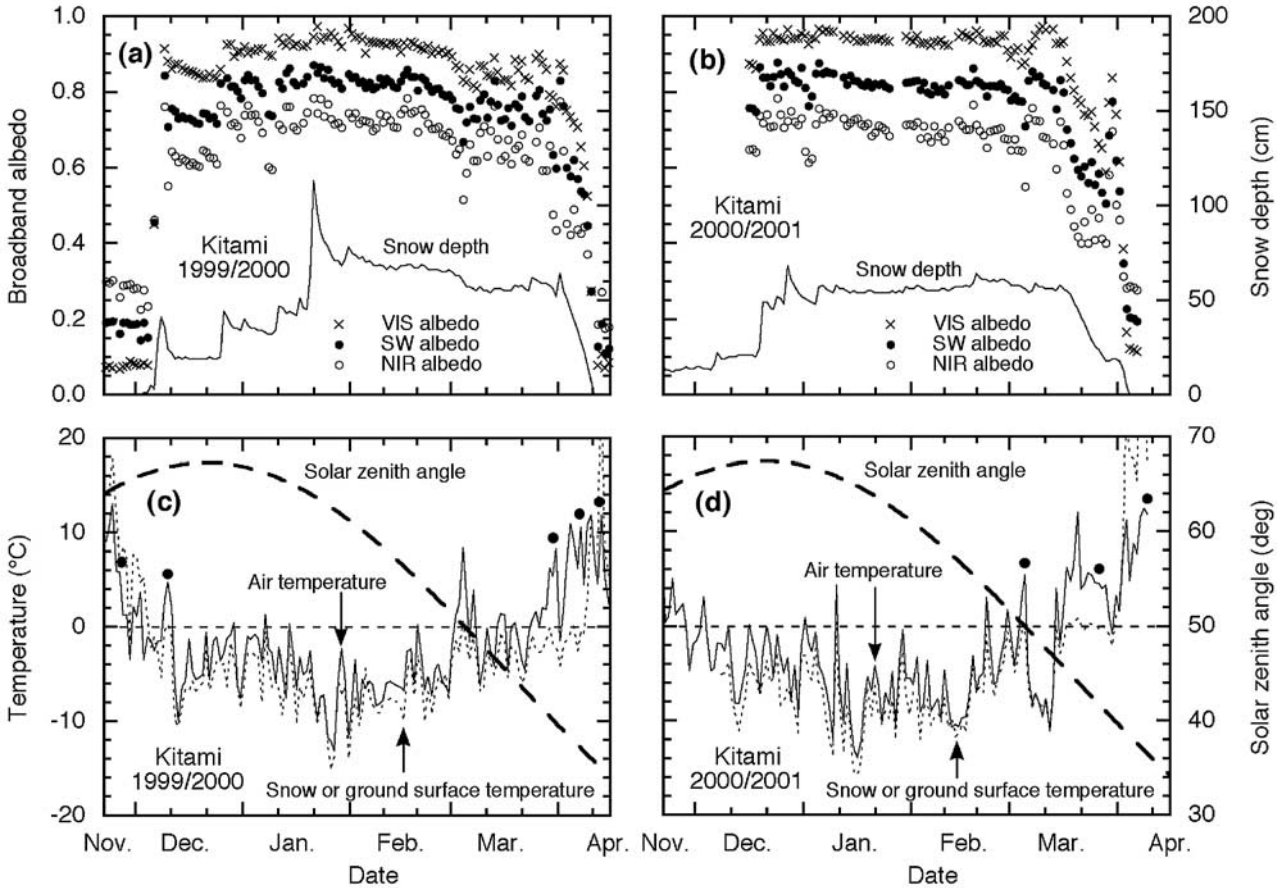

Figure 2. Daily variations of the visible (VIS), shortwave (SW), and near infrared (NIR) albedos averaged from 1131 to 1200 LT, and snow depth at 1200 LT for (a) 1999/2000 winter and (b) 2000/2001 winter. Air temperature, snow surface/ground temperature, and solar zenith angle at 1200 LT for (c) 1999/2000 winter and (d) 2000/2001 winter. Dots above the curve of air temperature indicate rainfall.

daily variations of representative snow and meteorological components at 1200 LT (albedos were averaged in 1131–1200 LT) of every day during all observation periods. The maximum snow depth in the 1999/2000 was 117 cm and that in the 2000/2001 winter was 72 cm. The average snow depths in midwinter were around 60 cm. The air and snow temperatures were almost always negative in December, January, and February. When the surface was not covered by snow, the near infrared albedo was higher than the visible one. However, this relationship was reversed for the snow surface because of the difference in spectral variation of the albedo between withered grass and snow cover. Snow albedos vary with small variations of snow depth, which we will examine in detail in the next section. Snow began to melt in March and disappeared in April.

[11] Figure 3 shows the observed results of snow type obtained from snow pit work. Until the beginning of March when snow melting began, the snow consisted of dry snow such as new snow, faceted crystals, and depth hoar. We refer to this period as the "dry snow season" or "accumulation season." After the beginning of March, almost all snow layers consisted of wet snow (granular snow). We refer to this period as the "wet snow season" or "melting season." However, from the viewpoint of snow albedo, snow type in a few layers near the surface is important. In 2001, snow types in almost all snow layers changed to granular snow on 6 March. This is caused by the positive air temperature with rainfall on 3–4 March, when the albedo decreased rapidly as shown in Figures 2b and 2d. After this event, snowfall at low temperature increased the albedo. From 6–13 March, new snow and/or faceted crystals on the thick crust were observed as shown in Figure 3b and caused the high albedo shown in Figure 2b. Thus we treated this period as the dry snow season. Since the snow pit work was not performed every day, the first day of the wet snow season between each snow pit work is determined by the snow surface temperature. Accordingly, we defined the wet snow season as starting on 6 March in 2000 and 16 March in 2001.

4. Effects of the Snow Physical Parameters on Broadband Albedos

4.1. Snow Aging

[12] The snow aging effect on albedo is generally due to two reasons. The first is an increase of snow grain size caused by a metamorphosis of snow grains such as sintering or melting. The second is an increase of snow impurities caused by dry deposition of the atmospheric aerosols or by the sublimation/melting of surface snow. These two factors reduce the snow albedo in such a way that the near infrared

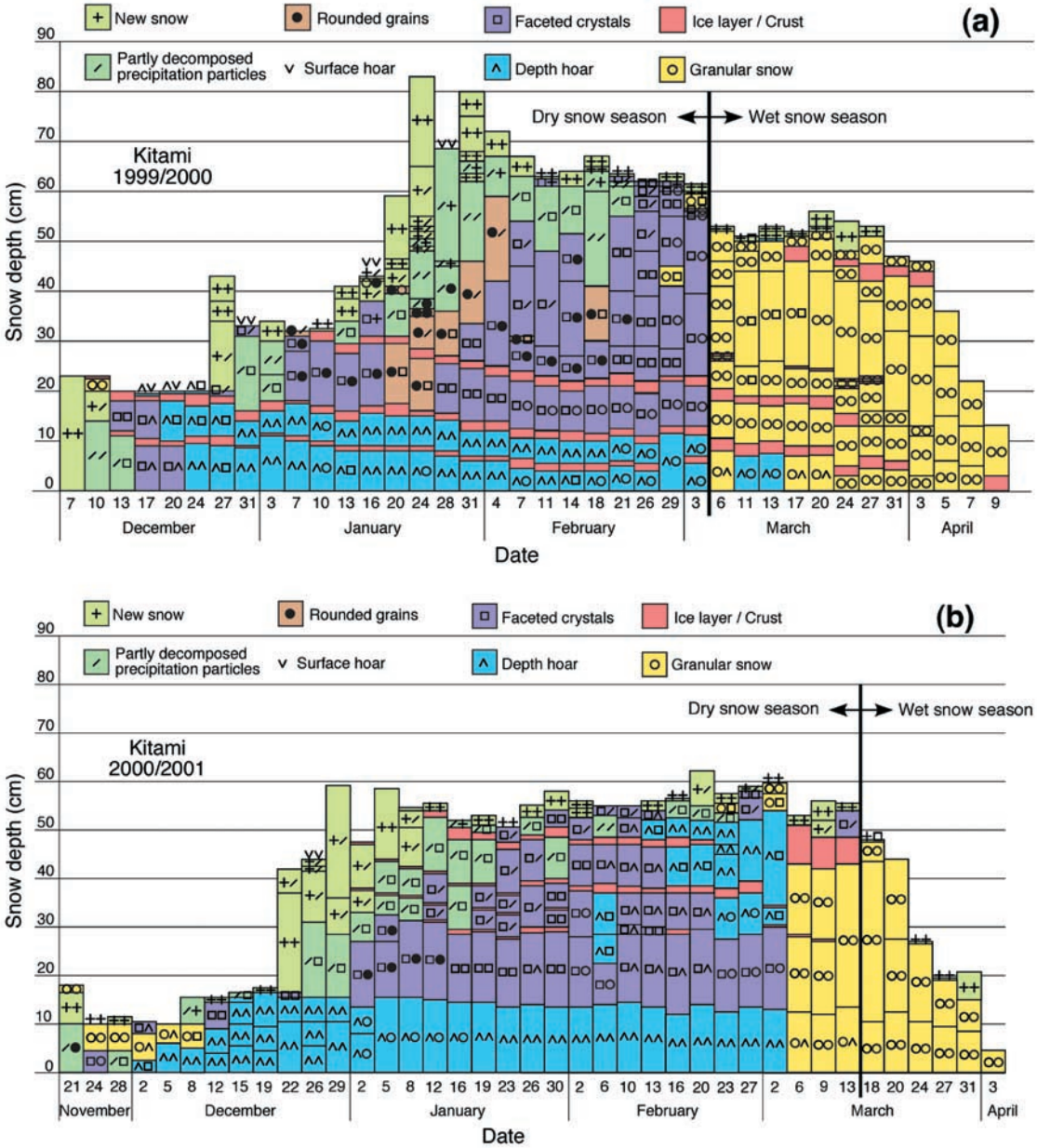

Figure 3. Snow pit work results showing the vertical profiles of snow types during (a) 1999/2000 winter and (b) 2000/2001 winter. Two major snow types are shown for each snow layer.

albedo mainly decreases with an increase of snow grain size and the visible albedo is reduced by snow impurities as described in section 1. In Figures 2a–2b, the broadband albedos increase with a steep increase of snow depth (i.e., snowfall), and decrease with elapsed time after snowfall. This is the snow aging effect. To see the detailed features of albedo reduction, three broadband albedos measured at local solar noon are plotted as a function of elapsed time after snowfall in Figure 4a, where we define a snowfall as an increase of snow depth exceeding 3 cm. Dots (plus symbols) indicate negative (positive) snow surface temperatures. The linear regression lines for each albedo are also plotted for negative and positive temperature ranges of snow surface, and the statistical parameters are shown in the upper part of Table 1. Figure 4a contains the effects of solar zenith angle and cloud cover on broadband albedos, which are discussed in Appendix A. Albedo reduction for positive snow surface temperature is remarkable, and it is larger for the near infrared region than for the visible region. This is because an increase of snow grain size is significant under positive snow surface temperatures. All correlation coefficients of the linear regression equation, however, are low as shown in Table 1. The effect of snow aging cannot be clearly classified by snow surface temperature.

[13] We next divided the observation period into the two parts of dry snow season and wet snow season as defined in Figure 3. As a result, the dependence of albedos on elapsed time after snowfall can be clearly classified as shown in Figures 4b and 4c. The correlation coefficients are also drastically increased, as shown in the lower part of Table 1. This means that the albedo of dry snow is stable because of small grain size under low temperature, while the albedo of

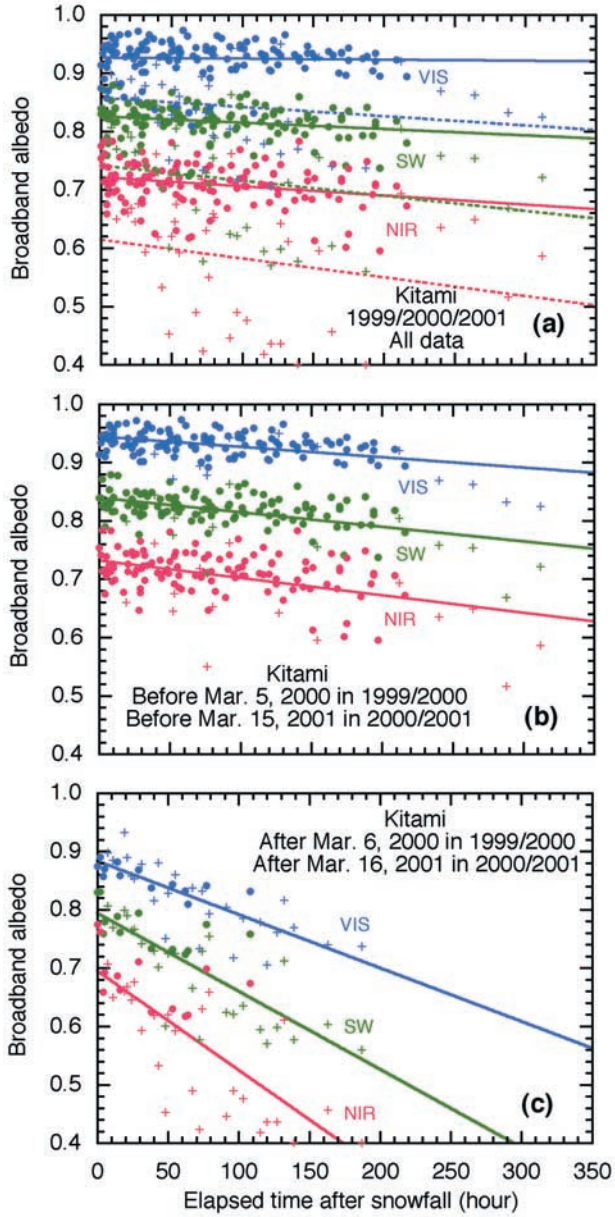

Figure 4. Broadband albedos in the visible, shortwave, and near infrared regions as a function of elapsed time after snowfall exceeding 3 cm for the period of (a) all data, (b) dry snow season, and (c) wet snow season. Dots (plus signs) indicate negative (positive) air temperatures. In Figure 4a the linear regression lines for each albedo are plotted for negative (positive) snow surface temperatures by solid (dashed) lines, and those in Figures 4b and 4c are plotted for negative and positive snow surface temperatures. The statistical parameters are shown in Table 1.

granular snow is relatively low and easily decreased because of large grain size and quick metamorphosis around the melting point. The dry deposition of atmospheric aerosols onto the snow surface is also masked by frequent snowfalls in the dry snow season (accumulation season). In the wet snow season (melting season), snow impurities appear at the snow surface by sublimation/melting of the surface snow. This effect accelerates the albedo reduction. However, we defined the "wet snow season" by an unusual method in section 3. If the "wet snow season" were defined by the ordinary method (i.e., determined only by the existence of granular snow), the correlation coefficients of the regression lines in Figure 4c would be very low. For this reason, it is generally difficult to calculate the snow albedo by elapsed time after snowfall in the wet snow season.

4.2. Snow Surface Temperature

[14] Both the snow aging effect and the air temperature (T_a) or snow surface temperature (T_S) are used in many empirical snow albedo models. We thus examined the relationship between the snow albedo and these temperatures based on all of our observed data including the snow albedos for snow depths of less than 30 cm and the ground albedo without snow. Figures 5a and 5b show the broadband albedos as functions of T_a and snow/ground surface temperature, respectively. In Figure 5a, the snow albedos gradually decrease at $T_a > 0°C$, while in Figure 5b, they drop drastically at positive snow/ground surface temperatures, where there are no high albedos. Figure 5b shows that the snow surface temperature never exceeds the melting point, but this is an important fact for empirical snow albedo models.

[15] Figure 6a shows the T_S dependence of shortwave albedo reduction after snowfall and the linear regression lines for each range of T_S. The statistical parameters are shown in Table 2. The albedo reduction with elapsed time after snowfall is very small at low T_S and increases with increasing T_S. However, it is very scattered for $T_S \geq -10°C$. This means that T_S is not a good parameter for predicting the snow albedo around the melting point where the snow albedo is affected both by the current T_S and by past meteorological conditions. Therefore we estimated the albedo reduction rate per day as a function of 24-hour mean snow surface temperature $\bar{T}_S$ (Figure 6b). The albedo reduction rate increases with $\bar{T}_S$ in the order of near infrared, shortwave, and visible regions. Although these values are also scattered, the results of significance testing for regression equations were all significant with a significance level of 99%, as shown in Table 2. This result implies that the albedo reduction rate due to snow aging statistically depends on snow surface temperature. However, it would

Table 1. Parameters of Statistic Analyses on Snow Albedos in Figure 4

Figure	Snow Condition	Spectral Region	Regression Coefficient a[a]	Regression Coefficient b[a]	Correlation Coefficient
4a	$T_s < 0°C$	VIS	1.79×10^{-5}	0.927	0.0341
4a	$T_s < 0°C$	SW	1.08×10^{-4}	0.826	0.211
4a	$T_s < 0°C$	NIR	1.57×10^{-4}	0.722	0.245
4a	$T_s \geq 0°C$	VIS	1.58×10^{-4}	0.858	0.180
4a	$T_s \geq 0°C$	SW	2.59×10^{-4}	0.741	0.233
4a	$T_s \geq 0°C$	NIR	3.21×10^{-4}	0.614	0.235
4b	dry snow season	VIS	1.78×10^{-4}	0.945	0.486
4b	dry snow season	SW	2.49×10^{-4}	0.840	0.528
4b	dry snow season	NIR	2.98×10^{-4}	0.732	0.452
4c	wet snow season	VIS	9.16×10^{-4}	0.883	0.792
4c	wet snow season	SW	1.34×10^{-3}	0.794	0.798
4c	wet snow season	NIR	1.70×10^{-3}	0.695	0.751

[a]Snow albedo is expressed by linear regression equation: $\alpha = -at + b$, where t is elapsed time after snowfall (hours) and a and b are regression coefficients.

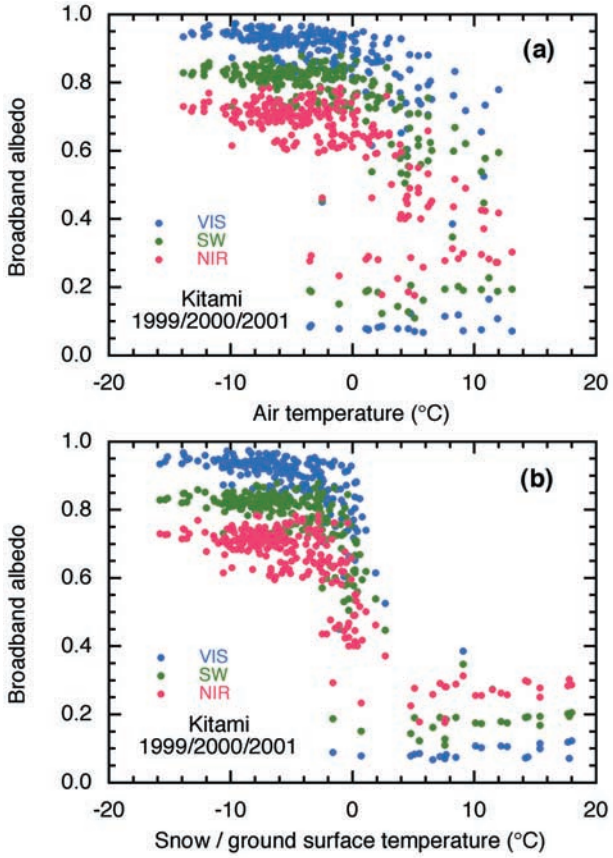

Figure 5. Broadband albedos as a function of (a) air temperature and (b) snow/ground surface temperature. Figure 5 includes snow albedos for snow depths of less than 30 cm and ground albedo without snow.

contain an error to some extent in snow albedo prediction using snow surface temperature.

4.3. Snow Grain Size and Snow Impurities

[16] Snow albedo essentially depends on snow grain size and snow impurities as mentioned in section 1 rather than on T_a or T_S. We investigated the effects of these snow physical parameters measured from snow pit work on broadband albedos. Figure 7 shows the broadband albedos as a function of snow grain size. Circles and crosses show the differences in the dimensions of measured snow grain sizes r_2 and r_3, as defined in section 2. Curves in Figure 7 show the theoretically calculated broadband albedos for several kinds of snow impurity concentrations (c), solar zenith angles (θ_0), and sky conditions (clear/cloudy). The effects of θ_0 and cloud cover on albedo are discussed in Appendix A. These curves represent the albedos under the possible variation ranges of c, θ_0, and cloud cover, when the snow albedo data we analyzed were measured. For example, for the visible region, the maximum albedo is theoretically expected under the conditions of c = 1 parts per million by weight (ppmw), $\theta_0 = 67°$, and clear skies, and the minimum albedo is theoretically expected under the conditions of c = 100 ppmw, $\theta_0 = 40°$, and clear sky (see Appendix A). We now look at the relationship between snow grain size and measured albedos in Figure 7, where the measured albedos decrease with the snow grain size, and decrease remarkably for the near infrared albedo. This tendency agreed with those of theoretically calculated albedos for the data of r_2, while the albedos for r_3 are lower than the theoretical ones. This means that the optically equivalent snow grain size is r_2 as shown by *Aoki et al.* [1998, 2000]. However, even for r_2, some data are out of the range of theoretically calculated albedos. One possible reason is that the light absorption is weak in the snow impurity model (OPAC mineral particles) we employed. We will discuss other possibilities later.

[17] It is worth showing the relationship between snow surface temperature and snow grain size, because the effect of temperature is important in its role in the growth of the snow grain size. Figure 8 shows this relation for r_2 and r_3, in which r_2 keeps small values at $T_S < -10°C$ and increases around melting point, while the value of r_3 is independent on T_S. The result of r_2 is consistent with the same figure estimated from satellite data by *Hori et al.* [2001]. However, the values of snow grain size at one fixed T_S widely distribute particularly for r_2 around melting point. This is because that snow grain size is determined not only by T_S at that moment, but also the past meteorological conditions such as T_S and incoming radiation.

[18] Figure 9 shows the broadband albedos as a function of concentration of snow impurities. Crosses, plus symbols, and circles show the differences in the sampling layer of

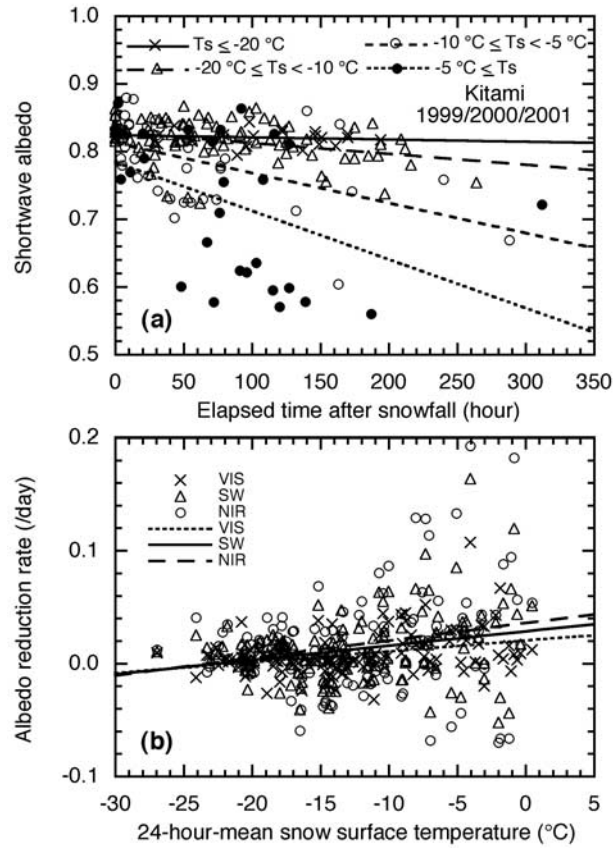

Figure 6. (a) Relationship of shortwave albedo with elapsed time after snowfall for four ranges of snow surface temperature. (b) Albedo reduction rate per day as a function of 24-hour mean snow surface temperature. The linear regression lines for each group of data are plotted. The statistical parameters are shown in Table 2.

Table 2. Parameters of Statistic Analyses on Snow Albedos in Figure 6

Figure	Snow Condition	Spectral Region	Regression Coefficients[a]	Correlation Coefficient	Significance Level, %
6a	$T_s < -20°C$	SW	$\alpha = -3.21 \times 10^{-5}t + 0.824$	0.144	>45
6a	$-20 \leq T_s < -10°C$	SW	$\alpha = -1.60 \times 10^{-4}t + 0.828$	0.341	>99
6a	$-10 \leq T_s < -5°C$	SW	$\alpha = -4.33 \times 10^{-4}t + 0.812$	0.506	>99
6a	$-5°C \leq T_s$	SW	$\alpha = -7.18 \times 10^{-4}t + 0.784$	0.448	>98
6b	all data	VIS	$r_\alpha = 9.61 \times 10^{-4}\bar{T}_s + 0.0203$	0.334	>99
6b	all data	SW	$r_\alpha = 1.27 \times 10^{-3}\bar{T}_s + 0.0285$	0.263	>99
6b	all data	NIR	$r_\alpha = 1.55 \times 10^{-3}\bar{T}_s + 0.0358$	0.229	>99

[a]Here α is snow albedo, t is elapsed time after snowfall (hours), r_α is albedo reduction rate per day, and $\bar{T}_S$ is 24-hour-mean snow surface temperature (°C).

snow. The measured albedos decrease with the concentration of snow impurities. *Warren and Wiscombe* [1985] showed the similar figures in which the theoretical calculated shortwave albedo is reduce by 10% by soot contained in snow of 0.1–1.0 ppmw depending on snow grain size, while the concentration of snow impurities begins to reduce the albedo in our measurement is higher roughly by 2 orders. This is due to the difference in absorptivity between soot and dust. In general, c is highest for the snow sampling layer of 0–1 cm depth, second for the layer of 0–5 cm depth, and lowest for the layer of 0–10 cm depth because the snow impurities are supplied by the dry deposition of the atmospheric aerosols, as described by *Aoki et al.* [2000]. Very high values of c, exceeding 100 ppmw, were recorded in the 0- to 1-cm layer as shown in Figure 9a, where the corresponding albedos fall in the theoretically calculated range. However, some of the visible albedos corresponding with c in the 0- to 10-cm layer were lower than any theoretical curve. Although this could also be explained by the weak absorption of the snow impurity model we employed, the nonhomogeneity of impurities (high at the top layer) in snow layers near the surface could reduce the visible albedo [*Aoki et al.*, 2000]. We will discuss this issue later. On the other hand, the measured near infrared albedos fall within the theoretically predicted range.

[19] In both the snow grain size dependence and the impurity dependence of broadband albedos, the measured albedos fall roughly in the theoretically predicted range. In general, when the snow grain size is large, the concentration of snow impurities is also high (i.e., the melting season). Moreover, there is an effect whereby a visible albedo reduction caused by snow impurities is enhanced by an increase of snow grain size [*Warren and Wiscombe*, 1980]. To examine the relationships among the measured values of these parameters and albedos, we plotted the broadband albedos as a function of c. We did this for several ranges of snow grain size as shown in Figure 10, where the measured value of c is for the 0- to 5-cm layer and the measured snow grain size is for r_2. The measured visible albedos in each range of snow grain size except for 500 μm $\leq r_2$ do not correspond with the theoretical curves. On the contrary, the measured near infrared albedos in each range of snow grain size have a clear correspondence with the theoretical curves. This is explained as follows: In the near infrared region, the light absorption by ice is stronger than that in the visible region, so the near infrared albedo contains the information of the snow physical parameters near the surface. The parameters of snow grain size and concentration of impurities were measured at the snow surface and in the 0- to 5-cm layer. This leads to the agreement of the measured near infrared albedo with the theoretical ones. In contrast, the visible albedo contains the information of the snow physical parameters in the relatively deeper snow layers. If the snow physical parameters in the deeper layers were not the same as the measured ones in the surface layers, the visible albedo would deviate from the theoretical curves. For example, if there were a new snow cover (small r_2) of a few centimeters on old granular snow (large r_2), the near infrared albedo would take a theoretically predicted value for small grain size. However, the visible albedo would be lower than the theoretically predicted value for all snow layers with small grain size due to the granular snow layer below. This issue of the measured albedos being lower than the theoretically calculated ones in the previous paragraph might also be related to the nonhomogeneity of the snow parameters.

[20] We measured the snow grain size throughout the snow layers and the concentration of impurities for three layers from the surface. These data looks useful to validate a relationship between visible albedo and snow physical parameters inside the snow. However, at the present stage it is practically difficult because of the following reasons: (1) The information of snow physical parameters such as grain size and impurities contained in visible albedo is the maximum at snow surface and decreases at lower layers. (2) Optical depth of snow layer per unit depth changes depending on parameters of snow density, grain size, and concentration of impurities. Therefore the effective layer of snow physical parameters related with the visible albedo themselves varies snow physical parameters. We should consider this problem as a future issue.

5. Conclusions and Outlook

[21] In land surface models or general circulation models, snow albedo is often predicted by means of empirical models. However, the snow albedo essentially depends on the snow physical parameters such as snow grain size and snow impurities. To obtain the basic data for improving the snow albedo model, we performed snow pit work at several-day intervals simultaneously with radiation budget observations during two winters in eastern Hokkaido, Japan. From these data, we investigated the effects of elapsed time after snowfall (snow aging), air temperature, and snow surface temperature, whose parameters are used in empirical snow albedo models, on the visible and the near infrared albedos. Using the radiative transfer model for the atmosphere-snow system, we calculated the effects of snow grain

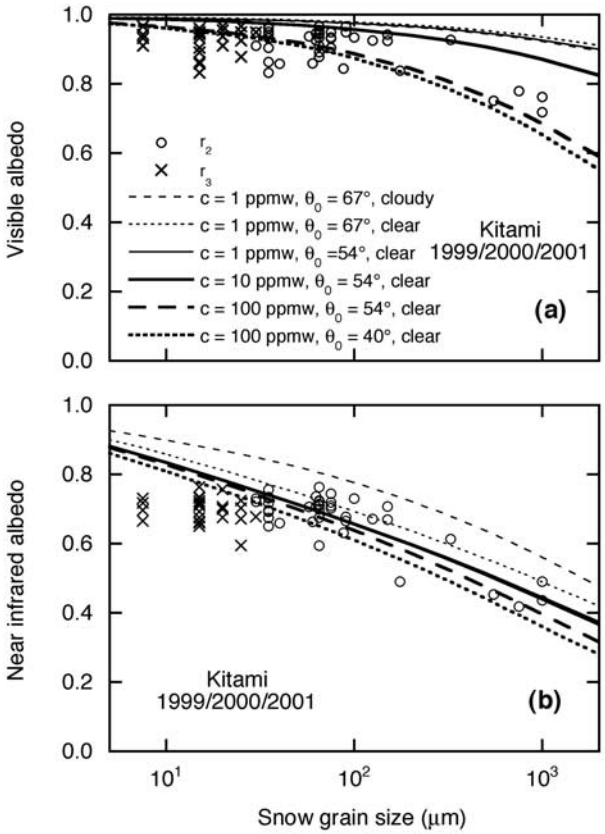

Figure 7. (a) Visible albedo and (b) near infrared albedo as a function of snow grain size. Circles and crosses show the differences in dimensions of measured snow grain size, r_2 and r_3 as defined in section 2. Curves show the theoretically calculated broadband albedos for several kinds of snow impurity concentrations (c), solar zenith angles (θ_0), and sky conditions (clear/cloudy).

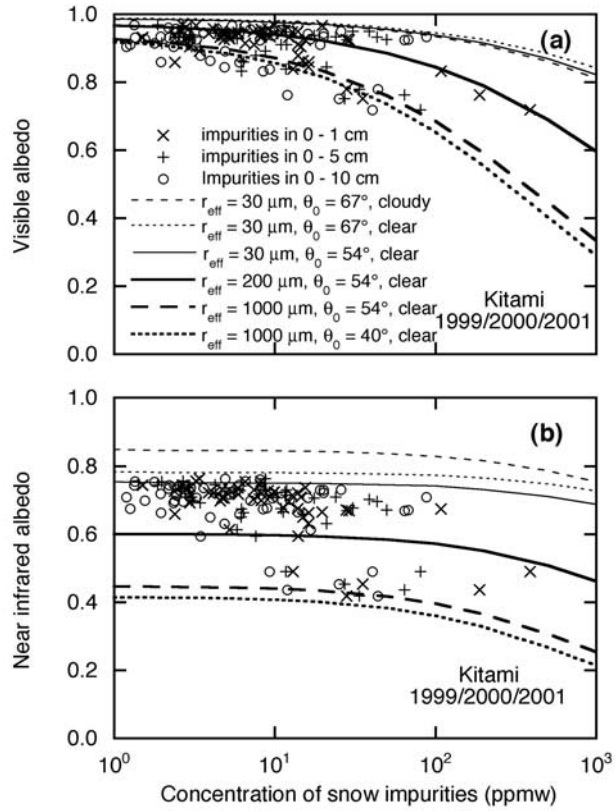

Figure 9. (a) Visible albedo and (b) near infrared albedo as a function of concentration of snow impurities (c). Crosses, plus signs, and circles show the differences in the snow sampling layer. Curves in Figure 9 show the theoretically calculated broadband albedos for several kinds of snow grain sizes (r_{eff}), solar zenith angles (θ_0), and sky conditions (clear/cloudy).

size and concentration of snow impurities on broadband albedos and compared them with the observed ones to develop a physically based snow albedo model in the future.

[22] The effect of snow aging on the broadband snow albedo could be seen in the scatterplot of albedos as a function of elapsed time after a snowfall greater than 3 cm. This dependence of albedo could be clearly classified by dividing the snow-covered periods into dry snow season and wet snow season. This result critically depends on the definition of the wet snow season. The albedo reduction by snow aging statistically depended on the snow surface temperature, which is often used to predict the snow albedo in the empirical model of the land surface process. However, the albedo reduction rate was very scattered for the snow surface temperature higher than −10°C. This is because the snow albedo reduction essentially depends on the snow grain size and the concentration of snow impurities.

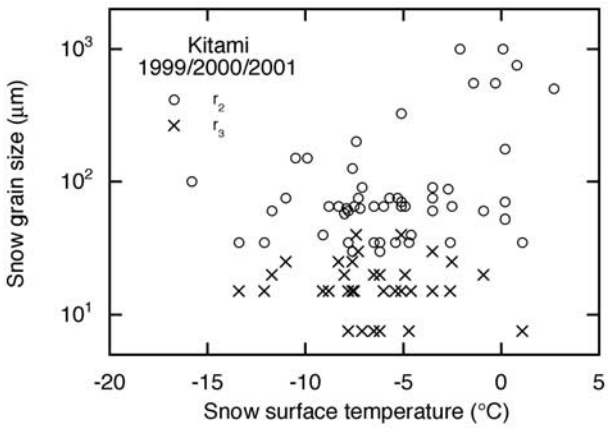

Figure 8. Relationship between snow surface temperature and snow grain size. Circles and crosses show the measured snow grain sizes of r_2 and r_3, respectively.

[23] Comparing measured snow albedos as functions of snow grain size and concentration of snow impurities with the theoretically calculated ones using the radiative transfer model revealed that the measured broadband albedos fell almost within the range of theoretically calculated ones. In particular, the measured near infrared albedos agreed well with the theoretical ones for the dependence on both snow grain size and impurities, while agreement with the visible albedo was not so good. This is due to the difference in light absorption by ice between the visible and near infrared regions. In the near infrared region, the light absorption by ice is strong and the albedo contains the information of the

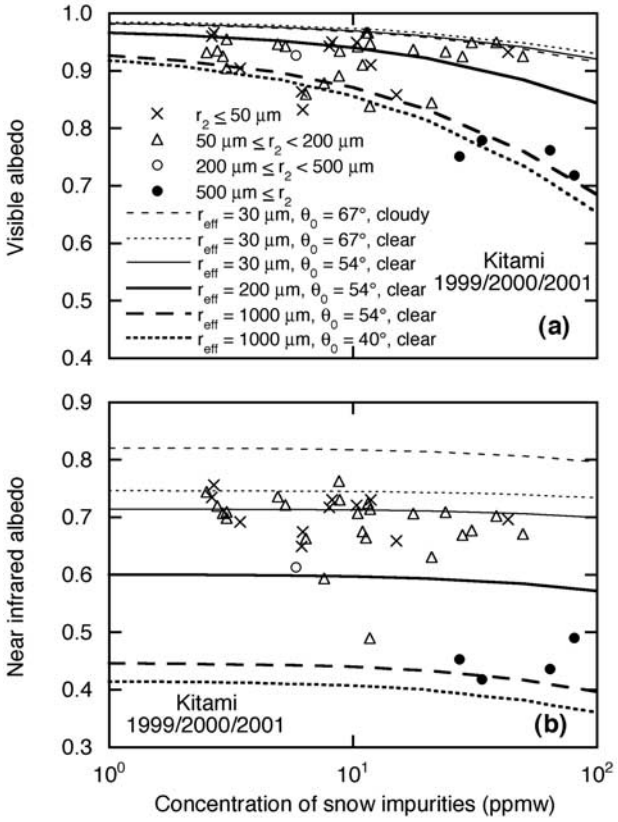

Figure 10. Same as Figure 9 but for the measured value of c in the 0- to 5-cm layer. Each value of measured albedos is plotted for four ranges of snow grain size (r_2).

snow physical parameters only near the surface where the parameters were measured. This led to a good agreement of albedos in this region. In contrast, the visible albedo contains the snow information in the deeper layer because the ice is relatively transparent in the visible region. This suggests the necessity of a multiple-snow-layer model in the visible region for the physically based snow albedo model.

[24] The surface condition in the cryosphere has changed in the past several decades and is expected to change more in the future. The physically based snow albedo model is thus necessary to accurately predict snow albedo, when the snow grain size and snow impurities are very important factors. *Hori et al.* [2001] demonstrated the preliminary results of satellite remote sensing of these snow parameters using MODIS data. This product would be useful to validate the future physically based snow albedo model. Furthermore, the issue of the multiple-snow-layer model for the visible albedo may be solved by the remote sensing technique using multiple spectral channels [*Li et al.*, 2001; *Tanikawa et al.*, 2002], which obtained information on the vertical profile of snow grain size by multiple spectral channels in the visible and near infrared regions.

[25] We discuss an applicability of our result to the other locations. Our observation site Kitami in Hokkaido is located in midlatitude and seasonal snow covered area. During the period from December to February, the air and snow temperatures were mostly negative even at local solar noon as shown in Figure 2, and the dry type snows were observed as shown in Figure 3. It is cold for its latitude and the normal (30 years) averaged minimum air temperatures in this period ranges from −9.8°C to −14.5°C. As shown in Figure 6, snow albedo was very stable for $T_S < -10$°C and decreased for $T_S \geq -5$°C. This tendency would be kept for the other sites. Particularly for the effect of snow grain size on albedo, the results at Kitami could be extended to the other areas. However, the absorptivity of snow impurities (i.e., dust or soot) and their amount vary depending on the locations. Since the concentration of snow impurities is very low in Antarctica [*Warren and Clarke*, 1990] and remote sea ice areas [*Warren and Clarke*, 1986], the snow aging effect on albedo related with snow impurities in these areas would be weaker than that in the present study.

[26] We finally discuss how best to use our result for improvement of snow albedo parameterization. Two parameters of snow grain size and concentrations of snow impurities should be treated as predictors in physically based snow albedo model. For this purpose, the snow grain size should be explicitly predicted in snow layer models such as the Crocus model [*Brun et al.*, 1992] and the SNOWPACK model [*Lehning et al.*, 2002], in which snow metamorphosis is calculated from the heat budget in the snow. For the concentration of snow impurities, in the model of *Marshall and Oglesby* [1994] it could be considered explicitly, but they assumed the pure snow in their paper. Since a source of snow impurities is the atmospheric aerosols, it is necessary to simulate both the process of transportation of the atmospheric aerosols (particularly soot and dust independently) and the deposition of atmospheric aerosols into snow. For validations of these processes, our result would give basic information. Our result would also be useful for the validation of empirical snow albedo models.

Appendix A: Theoretically Predicted Variability of Broadband Albedos

[27] Broadband albedos were calculated to examine the effects of the solar zenith angle (θ_0) and cloud cover using a multiple scattering model of radiative transfer for the atmosphere-snow system [*Aoki et al.*, 1999, 2000]. Figure A1 shows the visible and near infrared albedos under clear and cloudy skies as a function of θ_0. In this calculation, we used the model atmosphere of midlatitude winter, rural aerosol model with an optical thickness of 0.1 at a wavelength of λ = 0.5 μm, and the same model of water cloud as *Aoki et al.* [1999]. The atmosphere is divided into 14 layers, and the snow is treated as one layer, which means that physical parameters of snow are uniform from the surface to the bottom. Since the effects of θ_0 and cloud cover on albedos differ depending on the effective snow grain size (r_{eff}) and concentration of snow impurities (c), albedos are calculated for r_{eff} = 30 μm (new snow) and 1000 μm (granular snow), and c = 1 ppmw (background level) and 100 ppmw (very dirty case) of mineral particles as mentioned below. These values were determined from our snow pit measurements of r_2 for snow grain size and the concentration of impurities in the snow layer of 0–5 cm depth. For the size distribution of snow particles, we employed a lognormal distribution with a geometric standard deviation of 1.6 measured by *Grenfell and Warren* [1999] in Antarctica. For snow impurities, the coagulation mode of the mineral aerosol model [*Hess et al.*, 1998] was used because

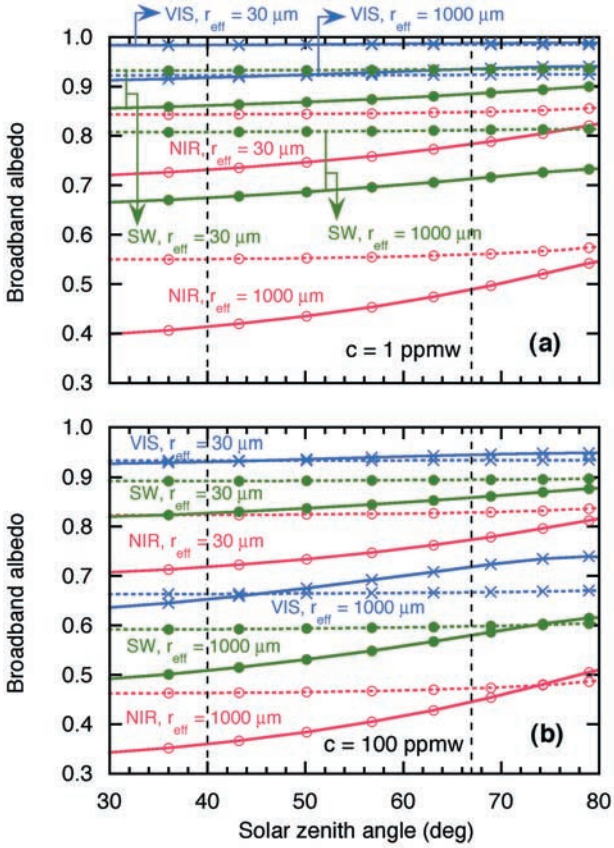

Figure A1. Theoretically calculated broadband albedos as a function of solar zenith angles under the conditions of r_{eff} = 30 and 1000 μm, clear sky (solid lines) and cloudy sky (dashed lines) and (a) c = 1 ppmw and (b) c = 100 ppmw.

the main constituent of snow impurities collected on the Nuclepore filter from our snow sample was mineral particles as mentioned in section 2. In Figure A1, the two vertical dashed lines indicate the maximum and minimum values of θ_0 varied in the observation period (at local solar noon from 1 December to 1 April, see Figures 2c and 2d).

[28] Comparing Figures A1a and A1b, we found that the visible albedo is reduced by an increase of c and that the degree of reduction is considerable for large r_{eff}. The effect of c is also seen on the near infrared albedo, where its reduction is 0.01 to 0.02 for r_{eff} = 30 μm and 0.06 to 0.09 for r_{eff} = 1000 μm from the case of c = 1 ppmw to the case of c = 100 ppmw. The effect of r_{eff} is significant for the near infrared albedo irrespective of the value of c. The combination of large values of r_{eff} and c reduces the visible albedo as mentioned above. The θ_0 dependence of snow albedo is generally significant for large r_{eff} and high c under clear skies in the near infrared region. In contrast, cloud cover eliminates the θ_0 dependence of albedos but increases the near infrared albedo for the reason mentioned in section 1. Therefore the maximum near infrared albedo appears under cloudy conditions, and the maximum visible albedo appears under clear conditions at θ_0 = 67°. The minimum albedo appears under clear conditions at θ_0 = 40° both for the visible and near infrared regions. Shortwave albedo shows middle behavior between the visible and near infrared albedos.

[29] **Acknowledgments.** This work was conducted as part of the ADEOS II/GLI Cal/Val experiment supported by the National Space Development Agency of Japan. We would like to thank Kimiteru Sado and Takashi Nakao for the use of the Observation Field in Kitami Institute of Technology. We also thank Hiroyuki Enomoto for his useful comments on the field observation. Discussions with Masashi Fukabori, Kazuo Mabuchi, Takeshi Yamazaki, and Hiroki Motoyoshi were beneficial for this study.

References

Aoki, T., T. Aoki, M. Fukabori, Y. Tachibana, Y. Zaizen, F. Nishio, and T. Oishi, Spectral albedo observation on the snow field at Barrow, Alaska, *Polar Meteorol. Glaciol.*, *12*, 1–9, 1998.

Aoki, T., T. Aoki, M. Fukabori, and A. Uchiyama, Numerical simulation of the atmospheric effects on snow albedo with a multiple scattering radiative transfer model for the atmosphere-snow system, *J. Meteorol. Soc. Jpn.*, *77*, 595–614, 1999.

Aoki, T., T. Aoki, M. Fukabori, A. Hachikubo, Y. Tachibana, and F. Nishio, Effects of snow physical parameters on spectral albedo and bidirectional reflectance of snow surface, *J. Geophys. Res.*, *105*, 10,219–10,236, 2000.

Brun, E., P. David, M. Sudul, and G. Brunot, A numerical model to simulate snow-cover stratigraphy for operational avalanche forecasting, *J. Glaciol.*, *38*, 13–22, 1992.

Dai, Y., et al., The common land model, *Bull. Am. Meteorol. Soc.*, *84*, 1013–1023, 2003.

Dickinson, R. E., A. Henderson-Sellers, and P. J. Kennedy, Biosphere-Atmosphere Transfer Scheme (BATS) for the NCAR Community Climate Model, *NCAR Tech. Note NCAR/TN-275+STR*, 69 pp., Natl. Cent. for Atmos. Res., Boulder, Colo., 1986.

Dickinson, R. E., A. Henderson-Sellers, and P. J. Kennedy, Biosphere Atmosphere Transfer Scheme (BATS) Version 1e as coupled to the NCAR Community Climate Model, *NCAR Tech. Note NCAR/TN-387+STR*, 72 pp., Natl. Cent. for Atmos. Res., Boulder, Colo., 1993.

Grenfell, T. C., and S. G. Warren, Representation of a nonspherical ice particle by a collection of independent spheres for scattering and absorption of radiation, *J. Geophys. Res.*, *104*, 31,697–31,709, 1999.

Hess, M., P. Koepke, and I. Schult, Optical properties of aerosols and clouds: The software package OPAC, *Bull. Am. Meteorol. Soc.*, *79*, 831–844, 1998.

Hori, M., T. Aoki, K. Stamnes, B. Chen, and W. Li, Preliminary validation of the GLI algorithms with MODIS daytime data, *Polar Meteorol. Glaciol.*, *15*, 1–20, 2001.

Intergovernmental Panel for Climate Change (IPCC), *Climate Change 2001*: *The Scientific Basis*: *Contribution of Working Group I to the Third Assessment Report of the Intergovernmental Panel on Climate Change*, edited by J. T. Houghton et al., 881 pp., Cambridge Univ. Press, New York, 2001.

Johannessen, O. M., M. Miles, and E. Bjorgo, The Arctic's shrinking sea ice, *Nature*, *376*, 126–127, 1995.

Jones, P. D., T. J. Osborn, K. R. Briffa, C. K. Folland, E. B. Horton, L. V. Alexander, D. E. Parker, and N. A. Rayner, Adjusting for sampling density in grid box land and ocean surface temperature time series, *J. Geophys. Res.*, *106*, 3371–3380, 2001.

Kondo, J., and H. Yamazawa, Measurement of snow surface emissivity, *Boundary Layer Meteorol.*, *34*, 415–416, 1986.

Lehning, M., P. Bartelt, B. Brown, C. Fierz, and P. Satyawali, A physical SNOWPACK model for the Swiss avalanche warning: Part II. Snow microstructure, *Cold Reg. Sci. Technol.*, *35*, 147–167, 2002.

Li, W., K. Stamnes, B. Chen, and X. Xiong, Snow grain size retrieved from near-infrared radiances at multiple wavelengths, *Geophys. Res. Lett.*, *28*, 1699–1702, 2001.

Liljequist, G. H., Energy exchange of an Antarctic snow-field: A, short-wave radiation, B, long-wave radiation and radiation balance, in *Norwegian-British-Swedish Antarctic Expedition, 1949–52, Scientific Results*, vol 2, part 1, 184 pp., Norsk Polarinst., Oslo, 1956.

Mabuchi, K., Y. Sato, H. Kida, N. Saigusa, and T. Oikawa, A biosphere-atmosphere interaction model (BAIM) and its primary verification using grassland data, *Pap. Meteorol. Geophys.*, *47*, 115–140, 1997.

Marshall, S., and R. J. Oglesby, An improved snow hydrology for GCMs. part 1: Snow cover fraction, albedo, grain size, and age, *Clim. Dyn.*, *10*, 21–37, 1994.

Nolin, A. W., and A. Frei, Remote sensing of snow and characterization of snow albedo for climate simulations, in *Remote Sensing and Climate Modeling*: *Synergies and Limitations*, edited by M. Beniston and M. M. Verstraete, pp. 159–180, Kluwer Acad., Norwell, Mass., 2001.

Parkinson, C. L., D. J. Cavalieri, P. Gloersen, H. J. Zwally, and J. C. Comiso, Arctic sea ice extents, areas, and trends, 1978–1996, *J. Geophys. Res.*, *104*, 20,837–20,856, 1999.

Robinson, D. A., Hemispheric snow cover and surface albedo for model validation, *Ann. Glaciol.*, *25*, 241–245, 1997.

Roesch, A., H. Gilgen, M. Wild, and A. Ohmura, Assessment of GCM simulated snow albedo using direct observations, *Clim. Dyn.*, *15*, 405–418, 1999.

Sellers, P. J., Y. Mintz, Y. C. Sud, and A. Dalcher, A Simple Biosphere model (SiB) for use within general circulation models, *J. Atmos. Sci.*, *43*, 505–531, 1986.

Takayabu, I., K. Tanaka, T. Yamazaki, K. Ueno, H. Yabuki, and S. Haginoya, Comparison of the four land surface models driven by a common forcing data prepared from GAME/Tibet POP'97 products—Snow accumulation and soil freezing processes, *J. Meteorol. Soc. Jpn.*, *79*, 535–554, 2001.

Tanikawa, T., T. Aoki, and F. Nishio, Remote sensing of snow grain-size and impurities from Airborne Multispectral Scanner data using a snow bidirectional reflectance distribution function model, *Ann. Glaciol.*, *34*, 74–80, 2002.

Yamazaki, T., A one-dimensional land surface model adaptable to intensely cold regions and its applications in eastern Siberia, *J. Meteorol. Soc. Jpn.*, *79*, 1107–1118, 2001.

Yang, Z. L., R. E. Dickinson, A. Robock, and K. Y. Vinnikov, Validation of the snow submodel of the biosphere-atmosphere transfer scheme with Russian snow cover and meteorological observational data, *J. Clim.*, *10*, 353–373, 1997.

Warren, S. G., Optical properties of snow, *Rev. Geophys.*, *20*, 67–89, 1982.

Warren, S. G., and A. D. Clarke, Soot from arctic haze: Radiative effects on the Arctic snowpack, *Glaciol. Data*, *18*, 73–77, 1986.

Warren, S. G., and A. D. Clarke, Soot in the atmosphere and snow surface of Antarctica, *J. Geophys. Res.*, *95*, 1811–1816, 1990.

Warren, S. G., and W. J. Wiscombe, A model for the spectral albedo of snow, II: Snow containing atmospheric aerosols, *J. Atmos. Sci.*, *37*, 2734–2745, 1980.

Warren, S. G., and W. J. Wiscombe, Dirty snow after nuclear war, *Nature*, *313*, 467–470, 1985.

Wiscombe, W. J., and S. G. Warren, A model for the spectral albedo of snow, I: Pure snow, *J. Atmos. Sci.*, *37*, 2712–2733, 1980.

Zeng, X., M. Shaikh, Y.-J. Dai, R. E. Dickinson, and R. Myneni, Coupling of the common land model to NCAR community climate model, *J. Clim.*, *15*, 1832–1854, 2001.

T. Aoki, Meteorological Research Institute, 1-1 Nagamine, Tsukuba, Ibaraki 305-0052, Japan. (teaoki@mri-jma.go.jp)

A. Hachikubo, New Energy Resources Research Center, Kitami Institute of Technology, 165 Koencho, Kitami 090-8507, Japan. (hachi@snow2.civil.kitami-it.ac.jp)

M. Hori, Earth Observation Research Center, Japan Aerospace Exploration Agency, 1-8-10 Harumi, Cyuoku, Tokyo 104-6023, Japan. (hori@eorc.nasda.go.jp)